Geophysical Research Letters

RESEARCH LETTER
10.1029/2023GL106323

Along-Arc Volcanism in the Western and Central Aleutian From 2015 to 2021 Revealed by Cloud-Based InSAR Processing

Jiahui Wang[1], Zhong Lu[1], David Bekaert[2], Charlie Marshak[2], Marin Govorcin[2], Simran Sangha[2], Joseph Kennedy[3], and Patricia Gregg[4]

[1]Southern Methodist University, Dallas, TX, USA, [2]Jet Propulsion Laboratory, California Institute of Technology, Pasadena, CA, USA, [3]Alaska Satellite Facility, University of Alaska Fairbanks, Fairbanks, AK, USA, [4]University of Illinois at Urbana-Champaign, Champaign, IL, USA

Key Points:

- Cloud-based interferometric synthetic aperture radar production and time-series analysis framework is developed to map volcanic deformation in the western and central Aleutian
- Temporal and spatial behaviors of the deformation at more than 15 volcanoes are interpreted as a result of variations in tectonic settings
- Deformation at Tanaga, Great Sitkin and Yunaska volcanoes is discovered, and the corresponding magmatic/tectonic source is modeled

Supporting Information:

Supporting Information may be found in the online version of this article.

Correspondence to:

J. Wang,
jiahuiwang@smu.edu

Citation:

Wang, J., Lu, Z., Bekaert, D., Marshak, C., Govorcin, M., Sangha, S., et al. (2023). Along-arc volcanism in the western and central Aleutian from 2015 to 2021 revealed by cloud-based InSAR processing. *Geophysical Research Letters*, *50*, e2023GL106323. https://doi.org/10.1029/2023GL106323

Received 11 SEP 2023
Accepted 19 NOV 2023

Abstract Leveraging a cloud-based interferometric synthetic aperture radar time-series processing framework, we map the surface deformation along the western and central Aleutian volcanoes from 2015 to 2021. The observed crustal deformation from more than 15 volcanoes is attributed to a wide range of magmatic or tectonic processes, for example, magma accumulation in the magmatic reservoir, steady cooling or degassing of magma or hydrothermal systems, and faulting. More vigorous magmatism in the central Aleutian is noticed and appears to be related to higher magma production rates or higher magma ascent rates as a result of oblique subduction. New deformation patterns never observed in previous studies are detected and modeled at Tanaga, Great Sitkin and Yunaska. This study showcases the cloud-processing capability to generate interferograms at scale and processing tools to analyze these time series over large, tectonically active areas.

Plain Language Summary Surface deformation mapping plays a critical role in the study of volcanic systems, which helps reveal the status of the fundamental magmatic process, for example, magma transportation and stress accumulation. In this study, a new framework integrating cloud-based interferometric synthetic aperture radar (InSAR) products, that is, the Advanced Rapid Imaging and Analysis Sentinel-1 Geocoded Unwrapped Interferograms (ARIA S1 GUNWs), and time-series processing tools, are used to map the deformation history of the volcanoes in the western and central Aleutian from 2015 to 2021. Active deformation has been identified from more than 15 volcanoes during the investigation period, which are attributed to be consequences of a wide range of magmatic or tectonic processes. Temporal and spatial behaviors of the deformation patterns are interpreted as a result of variations in tectonic settings. New deformation patterns have been detected at Tanaga, Great Sitkin and Yunaska, which are further modeled using analytic models and are interpreted by different magmatic/tectonic sources. This study has demonstrated the capabilities of the new cloud-based framework for scalable generation of standardized InSAR products and rapid time-series deformation analysis.

1. Introduction

The western and central Aleutian volcanic arc, accommodating more than 20 active volcanoes (Figure 1), is one of the most volcanically and seismically active areas in the world. Volcanic deformation with diverse patterns has been identified at multiple sites in the western and central Aleutian since the 1990s, reflecting complex magmatic processes occurring in the volcanic system. Okmok and Seguam are periodically inflating and subsiding in response to magma intrusion and withdrawal (Lee et al., 2013; Lu et al., 2010). Persistent surficial subsidence has been detected at Kanaga and Amukta as a result of the cooling of erupted deposits (Lu & Dzurisin, 2014). Persistent subsidence with deeper sources produced by magma or hydrothermal cooling or degassing is observed at Fisher and Aniakchak (Gong et al., 2015; Kwoun et al., 2006). Surface deformation can also be absent from InSAR observations prior to eruptions at open-conduit volcanoes like Cleveland and Shishaldin (Wang et al., 2015).

InSAR measures the two-dimensional deformation field at promising temporal and spatial resolution, providing comprehensive details on the deformation field from a broad view. Previous InSAR deformation studies on the Aleutian volcanoes are generally limited to single or multiple volcanoes due to the restriction of data quality, and computation and processing complexities (Lu & Dzurisin, 2010; Lu et al., 2003; Wang et al., 2015); an

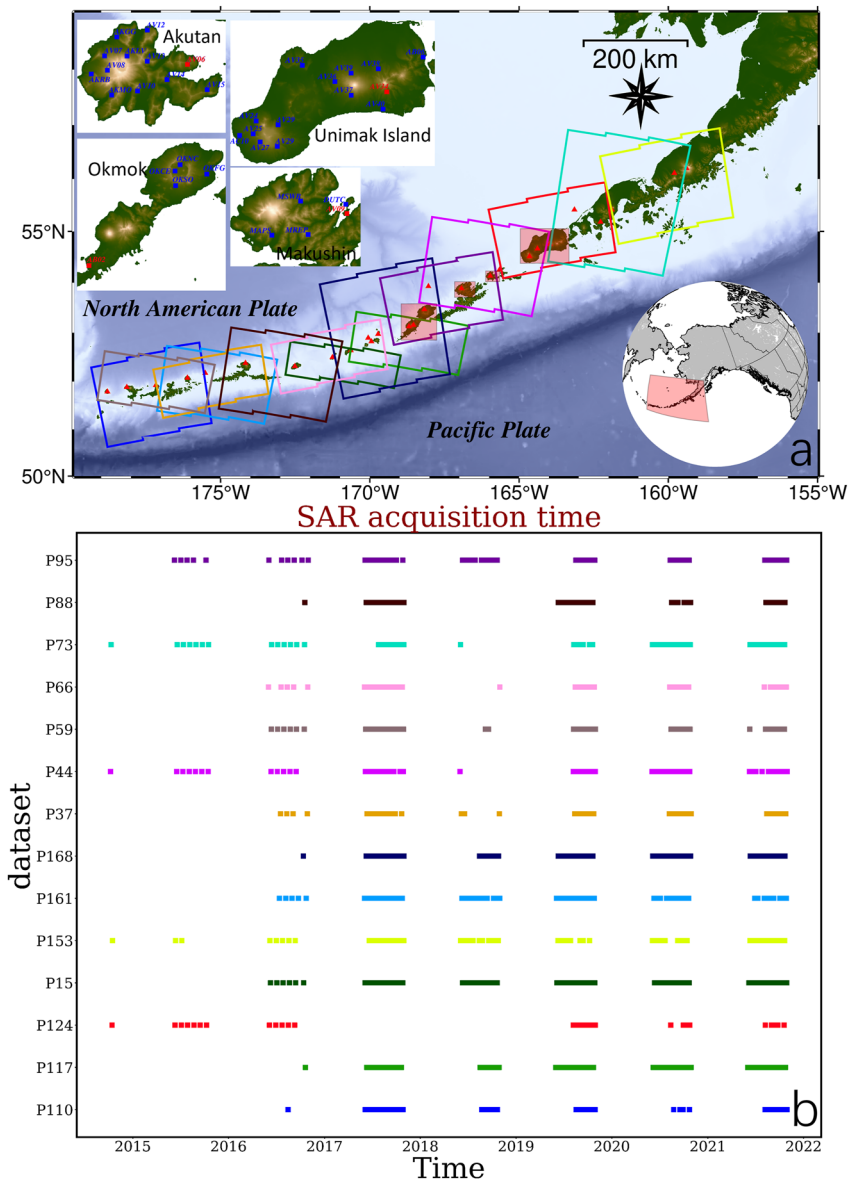

Figure 1. (a) Spatial coverage of the Sentinel-1 SAR acquisitions used for deformation mapping in the western and central Aleutian. Historically active volcanoes are marked with red triangles. Solid line boxes are the footprints of the ARIA S1-GUNW frames, colored by track names in (b) Insets are the four locations, that is, Okmok, Makushin, Akutan, and Unimak Island, used for validation of the derived InSAR results, using the continuous GNSS stations (blue squares) and reference stations (red squares). (b) Temporal distribution of the SAR data.

arc-wide deformation survey took several years (Lu & Dzurisin, 2014). Instead, our study aims at rapid mapping of the arc-wide volcanic deformation since 2015 by leveraging the cloud-based InSAR processing capabilities to evaluate the status of the volcanic activities in the western and central Aleutian. In partnership with JPL's Advanced Rapid Imaging and Analysis (ARIA) project and the Alaska Satellite Facility (ASF), we used the ARIA- Hybrid Pluggable Processing Pipeline (HYP3) InSAR processing framework to produce a dense time series with Sentinel-1 Synthetic Aperture Radar (SAR) acquisitions from 2015 to 2021.

Our ARIA-HyP3 framework uses state-of-the-art InSAR processing algorithms (i.e., InSAR Scientific Computing Environment 2, ISCE2; Rosen et al., 2012) to generate standardized sensor-neutral products (i.e., the ARIA-S1-GUNWs; Bekaert et al., 2019), that are then published to the ASF Distributed Active Archive Center (DAAC), where they are stored and are freely available for download. This significantly simplifies the processing

workflow by reducing the redundant exertion of interferogram generation on the user side. Cloud-compatible tools such as OpenSARlab (Meyer et al., 2021) allow the possibility to run data accessing and processing within the cloud alongside the ASF DAAC InSAR archive. The elimination of the need for data downloading improves processing efficiency and diminishes the cost of data storage remarkably, especially for large-area applications. The generated InSAR displacement time series are validated by comparison with Global Navigation Satellite System (GNSS) observations. Temporal and spatial patterns of the crustal deformation are used to track the evolution of the along-arc volcanism and evaluate the interaction between regional tectonic environments and magmatism.

2. Data and Methods

ARIA S1-GUNW products generated from the Sentinel-1 A/B data sets are used to produce the line of sight (LOS) deformation time series for more than 20 volcanoes, from Mt. Gareloi in the west to Mt. Veniaminof in the east (Figure 1a). A total of ∼4,700 geocoded unwrapped interferograms are produced from SAR images acquired from 14 different satellite acquisition tracks (Figure 1b), spanning the observation period from 2015 to 2021. Only SAR data collected during summers from June to October are exploited for the analyses to avoid coherence loss induced by snow/ice coverage in winter (Lu & Dzurisin, 2014). Only SAR pairs in the neighboring summers are used to produce the ARIA GUNW products. The Sentinel-1 images acquired from ascending and descending orbits are processed within a multi-looked scheme to suppress the noise and improve the interferometric coherence (Lee et al., 1998). Look numbers of 7 and 19 in azimuth and range directions are used, respectively, which are standard ARIA processing parameters. The interferograms in radar coordinates are geocoded to geographic coordinates with 3 by 3 arc second resolution for further analysis.

InSAR measurements are prone to perturbation by multiple types of noise, for example, phase delay due to atmospheric phase screen (APS), phase ramp induced by baseline errors, and unwrapping errors caused by low coherence or phase discontinuities (Bekaert et al., 2015; Fattahi & Amelung, 2014; Li et al., 2009; Zhang et al., 2019). Some of the central Aleutian volcanoes are deployed with continuous GNSS (cGNSS) stations, which provide sustained observations of crustal movement (Blewitt et al., 2018). The derived InSAR time-series measurements are compared and validated with the cGNSS records at four locations (Okmok, Makushin, and Akutan volcanoes and Unimak Island; Figure 1a). A total of 36 stations maintained by the University of Alaska Fairbanks (UAF) and EarthScope are installed at these locations (Figure S1 in Supporting Information S1). All stations were operational during the observation period from 2015 to 2021 coinciding with the InSAR measurements, and stations are all covered in the coherent InSAR deformation maps, providing great test sites for our application.

The production of InSAR time-series deformation maps over the western and central Aleutian volcanoes is accomplished through two stages—the large-scale production of the ARIA S1-GUNW products and then the time series inversion with the multi-temporal InSAR stacks. We perform the time-series processing within the OpenSARlab. Layers of the ARIA GUNW products are extracted for time-series ingestion with the ARIA tools (Buzzanga et al., 2020; Sangha, 2021). Sentinel-1 tracks with multiple adjacent frames along the satellite track are stitched to generate seamless interferograms with complete spatial coverage. We leveraged the ARIA-tools virtual data processing which allows accessing of virtual files from uniform resource locator pointing to on-cloud data and data loading from memory to save computation resources. Due to the spatially segregated characteristics of the Aleutian Islands, pronounced phase jumps between islands may be introduced during phase unwrapping. We employ an island-wise processing strategy to avert this situation. Isolated islands with reliable relative measurements are detected and separated with Global Self-consistent Hierarchical High-resolution Shorelines (GSHHS) water mask. The separated islands are then used in subsequent analysis.

The open-source Miami InSAR Time-series software in Python (MintPy) (Zhang et al., 2019) is applied to reconstruct the surface displacement history based on Small Baseline Subset (SBAS) algorithm (Berardino et al., 2002). The SBAS network is designed to keep robust connectivity and maximize the common intersection of the connected components for each interferogram, which is a metric for the quality of phase unwrapping with SNAPHU (Chen & Zebker, 2002). Unwrapping error correction is applied using the bridging and phase closure methods (Zhang et al., 2019). APS effects are mitigated with PyAPS (Jolivet et al., 2011) using the ERA5 weather model. To validate the InSAR measurements, constant tectonic corrections are made to the cGNSS records at Okmok, Akutan, Makushin, and Unimak Island, by subtracting the measurements of stations located in regions with no volcanic deformation (Figure S1 in Supporting Information S1). The three-dimensional cGNSS records

are then projected to the LOS direction and compared with the InSAR measurements. The derived displacement time series at several volcanoes are used to model deformation source parameters using Geodetic Bayesian Inversion Software (GBIS) (Bagnardi & Hooper, 2018).

3. Results

Surface displacement histories in the LOS direction have been produced at 25 historically active volcanoes from 2015 to 2021 illuminating diverse spatial and temporal deformation patterns (Figure 2). Persistent surficial subsidence on the flanks of volcanoes or inside volcanic calderas is identified at Gareloi, Kanaga, Atka, Amukta, Cleveland and Pavlof, with amplitudes ranging from 0 to about 20 mm/yr. The spatial distributions of the subsidence are highly correlated with the surface lava flow and pyroclastic deposits produced by previous eruptions (Lu & Dzurisin, 2014), and have relatively stable subsidence rates. Persistent, caldera-centered subsidence with steady rates and spatial patterns produced from deeper processes are revealed at the western caldera (7.2, Figure 2) and eastern caldera (7.3, Figure 2) of Seguam, and Fisher caldera (21, Figure 2), with deflating rates of about 10, 5, and 10 mm/yr, respectively. Persistent dominant subsidence as well as minor uplift episodes have been recorded at the Atka volcanic center since 2016. Yunaska has been subsiding at a steady rate of about 20–30 mm/yr in the central caldera since 2016.

Caldera-wide inflations with time-varying rates and spatially stable distributions are revealed at Seguam, Okmok, Makushin, Akutan, and Westdahl. Rapid inflation at a rate of about 60–80 mm/yr is identified from the eastern caldera of Seguam from 2020 to 2021 (7.1). Episodic exponential uplifts have been observed from the central caldera of Okmok since 2015, with an average deformation rate larger than 70 mm/yr. An uplift episode with an average rate of about 10 mm/yr has been identified at Makushin covering the whole caldera from 2015 to 2018, followed by subsidence with a similar spatial scale. Multiple episodic inflation events with average rates at about 5 mm/yr are observed to the northeast of the Akutan caldera. Westdahl has been persistently inflating from the central caldera at a steady rate of about 10 mm/yr since 2015. Great Sitkin exhibits inflation between the 2018 and 2020 eruption, and then contraction in 2021.

Most of the deep-seated deformation can be reproduced with a single Mogi source, that is, a point source embedded in a homogeneous and isotropic elastic half space (Kiyoo, 1958). Deep-seated subsidence at Seguam, Amukta, Fisher, and Yunaska (Section 5.1) can be reproduced from Mogi sources located at a depth range of about 1,500–9,000 m BSL (Figure 2). Deformation at Atka and Makushin have the best-fit Mogi source located at a depth from about 3,000 to 7,000 m BSL (Figure 2). Inflation observations at the eastern caldera of Seguam, Okmok, Akutan, and Westdahl are produced by sources located about 4,000–7,000 km BSL (Figure 2). Inflation at Great Sitkin can be approximated by a Mogi source at a depth of about 5,000–7,000 m BSL (Section 5.2). Deformation at Tanaga can be fit by a strike-slip fault at a depth of about 4 km BSL (Section 5.3).

The general consistency between InSAR and cGNSS measurements, with root mean square (RMS) misfits of around or less than 1 cm at most stations, indicates that the InSAR results capture the volcanic deformation well (Figures 2b–2e and Figure S1 in Supporting Information S1). The notable deviation between InSAR and cGNSS at Okmok's OKCE is most likely a consequence of the decorrelation noise in regions with rapid deformation. It can be resolved by using data sets with higher spatial resolution and temporal sampling. The overall good agreements between the cGNSS and InSAR results validate the accuracy and robustness of the cloud-based time-series InSAR deformation mapping framework.

4. Temporal and Spatial Characteristics of the Along-Arc Volcanism

Diversities in temporal and spatial domains are the most pronounced characteristics of the deformation patterns in the western and central Aleutian volcanoes. Two major inflation patterns are identified - continuous inflation events produced from spatially steady sources at time-varying rates at Okmok, Akutan and Westdahl, and episodic inflation events that occur intermittently at Great Sitkin, Seguam, and Makushin. The persistent inflation events are the continuation of successive inflation periods that started prior to 2015, with similar source locations and depths (Lu et al., 2010; Wang et al., 2018, 2021; Xue & Freymueller, 2020). The inflating episodes detected at Seguam and Makushin are analogous to the ones in previous deformation surveys and are very likely produced from the same sources (Lee et al., 2013; Xue & Freymueller, 2020). The persistent inflation observations likely indicate continued magma supply to the existing magmatic reservoirs and are usually associated with

10.1029/2023GL106323

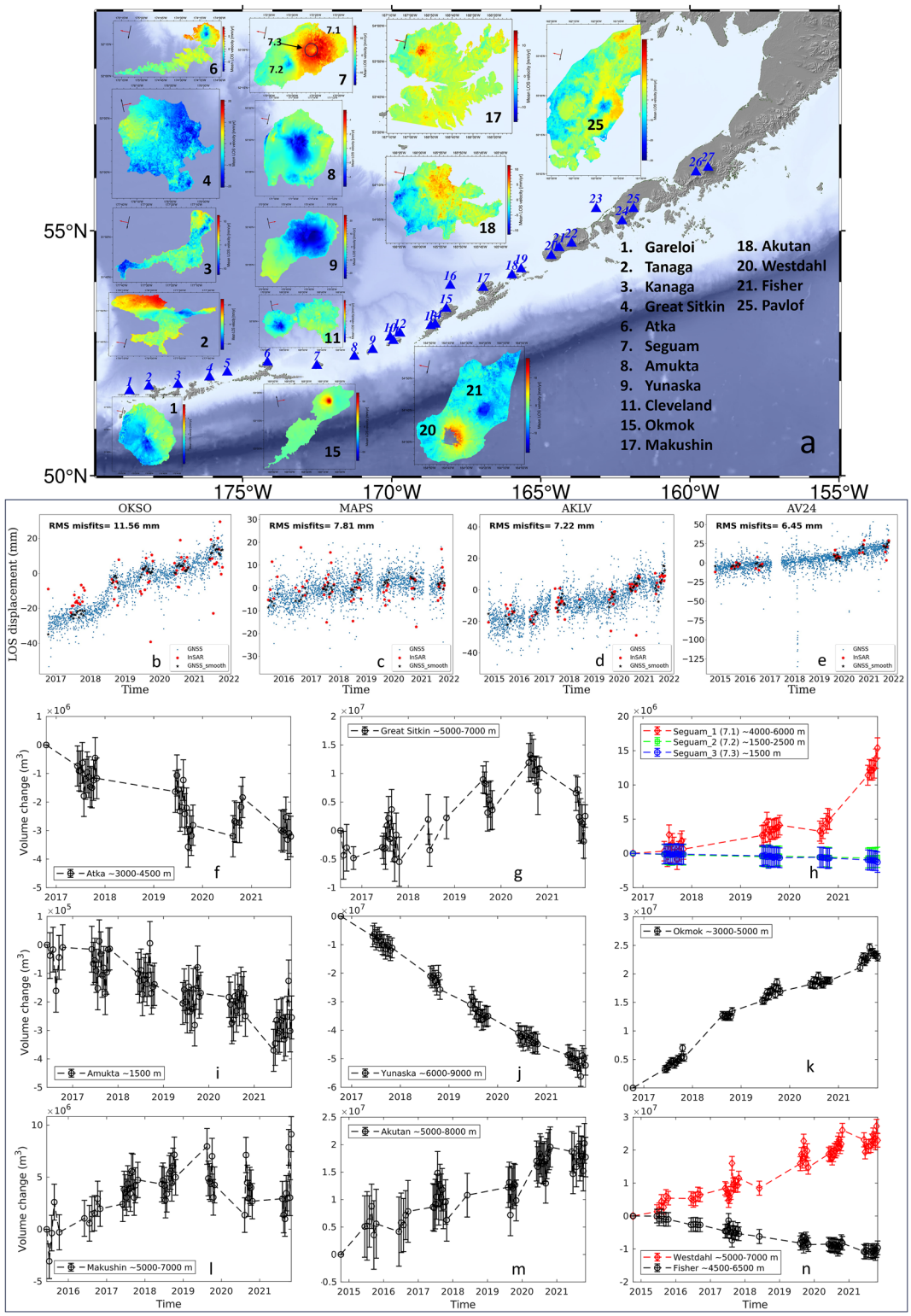

Figure 2. (a) Surface deformation velocity in LOS direction estimated from the Sentinel-1 acquisitions over the western and central Aleutian volcanoes. Color ranges are different for each volcano due to the wide range of velocities. The volcano's location is shown as the number tag. The three different deformations at Seguam, that is, eastern caldera, western caldera, and center of the eastern caldera, are labeled 7.1, 7.2, and 7.3, respectively. Volcanoes with no observed deformation or loss of interferometric coherence are not listed here. (b–e) Comparison between InSAR and GNSS measurements in the LOS direction at example GNSS stations shown in Figure 1a. Additional comparison results can be found in Figure S1 in Supporting Information S1. (f–n) Volume change histories at volcanoes with deep-seated inflation/deflation sources. The approximate depths of the Mogi sources are labeled.

more persistent temporal patterns while the episodic inflation episodes show more intermittent features and are typically suggestive of magma accumulations in stages. Despite the deficiency of effective deformation monitoring before the 1990s, persistent inflation events are only seen over the central Aleutians while episodic inflation is widely seen in both the western and central Aleutians. Temporally and spatially steady shallow deflations correlated to the emplaced lava flow and pyroclastic deposits are produced from thermoelastic contraction (Dzurisin et al., 2019; Lu & Dzurisin, 2014). Persistent deep-seated deflation observations are likely produced by degassing, viscoelastic relaxation, or contractional hydrothermal/magma cooling (Hamling et al., 2014; Lee et al., 2013; Lu & Dzurisin, 2014; Mann & Freymueller, 2003). Long-term subsidence at varying spatial scales is rather common in the western and central Aleutian. This is indicative of recent eruptive activity and active magmatic systems. The subsidence is usually accompanied by other volcanic deformation, for example, episodical inflations at Atka and Makushin. Volcanoes can also erupt without deforming the crust. Several eruptions have been produced from Cleveland, Shishaldin, and Pavlof during our observation period. However, no appreciable deformation was found associated with these eruptions. The absence of co-eruptive deformation has also been confirmed in previous observations, and is likely produced by open-conduit plumbing systems or deep magma reservoirs (Lu and Dzurisin). Eruptions without volcano-wide deformation are only observed in the central Aleutian, and are associated with much higher eruption frequency (Figure S2 in Supporting Information S1). Deformation at Tanaga is believed to be produced from strike-slip faulting (Section 5.3). Earthquake-induced crustal deformations are rarely observed in InSAR at volcanoes in the western and central Aleutian since volcanic-tectonic (VT) earthquakes are usually not big enough to produce crustal deformation appreciable to InSAR.

Significantly higher magma influx rates are observed in the central Aleutian, represented by the much larger volume accumulations from Okmok, Akutan, and Westdahl, as well as more frequent eruptions produced from Cleveland, Shishaldin and Pavlof during our observation period. The much higher magma influx rates are also consistent with the higher historic eruption frequency in the central Aleutian (Figure S2 in Supporting Information S1). A majority of the confirmed eruptions in the western and central Aleutian were produced from 7 volcanoes from Cleveland to Pavlof since about 1800s. Observations from volcanic CO_2 emissions, which have been measured 1 order of magnitude larger than those in the western Aleutian (Fischer et al., 2021), also agree with the high magma influx rate in the central Aleutian. The distinction in volcanism between the western and central Aleutian is likely a result of spatial variations in regional tectonics. The higher down-slip rates of the subducting Pacific Plate in the central Aleutian provide more water-rich sediments for the production of primitive magma from the partial melting of the mantle wedge (Buurman et al., 2014; DeMets et al., 1994; Kelemen et al., 2003; Kreemer et al., 2014). The dominant extensional tectonic setting created by probably the curvature of the arc may promote the magma ascent rate in the central Aleutian by providing a preferential pathway for magma migration (Magee et al., 2013; Ruppert et al., 2012).

5. Newly Discovered Deformation

5.1. Yunaska

Persistent caldera-wide deflation with a constant rate has been detected at Yunaska since 2015, where only surficial subsidence attributed to thermoelastic contraction of historically emplaced lava flows were detected in previous InSAR survey from 2004 to 2009 (Lu & Dzurisin, 2014). Our modeling results suggest a best-fit Mogi source located about 8 km beneath the center of the caldera, with an average volumetric change rate of about -58×10^6 m^3/yr (Figure S3 in Supporting Information S1). A wide variety of volcanic processes have been suggested to explain large-scale deep-seated surface deflation at volcanoes worldwide such as magma drainage from the reservoir during eruption (Geist et al., 2008; Lu & Dzurisin, 2010; Ofeigsson et al., 2011), viscoelastic relaxation of the crustal shell surrounding the magma chamber (Townsend, 2022), thermal contraction produced by magma/hydrothermal system cooling (Gong et al., 2015; Lee et al., 2013; Wang & Aoki, 2019), degassing or fluid loss (Nakaboh et al., 2003; Shreve et al., 2022; Trasatti et al., 2019). The most recent eruption recorded at Yunaska occurred in 1937, rejecting the co-eruptive deflation scenario (Lu & Dzurisin, 2014). Cooling-induced subsidence is typically initiated after the magma intrusion and can be persistent over a long time, in which case deflation should have also been detected in previous InSAR surveys. Degassing and fluid loss are usually associated with hydrothermal systems, yet no hot springs or active fumaroles are known to exist on Yunaska Island (avo.alaska.edu). One possible interpretation for the volume loss is magma or hydrothermal fluid drainage from the magmatic reservoir through fractures and accommodated by space produced in the crust by regional extensional

stress regime, which may also be responsible for the continuous deflation observed at Askja and Krafla volcanoes in Iceland (de Zeeuw-van Dalfsen et al., 2005; Rymer et al., 1998). Draining to a deeper level is not favorable for undegassed magma, for which horizontal sills are more likely to propagate (Tibaldi et al., 2010). Lateral or upward movement of mass in the plumbing system is expected to be associated with signals in the form of earthquake swarms or seismic tremors. Yunaska is among one of the most seismically quiescent islands in the Aleutian arc, no seismic anomaly coeval the deflation is detected. However, this hypothesis cannot be ruled out. The absence of seismic anomaly may be a result of the lack of nearby seismic stations as the nearest seismic stations are located on Herbert and Chuginadak Island in the east, with an average distance of about 50 km, which may not be able to detect the microseismicity produced during the magma/hydrothermal fluid transportation. Surface deformation is expected to be seen if magma migrates laterally or flows into shallow ponds in the scenario of incompressible magma and host rocks. While de Zeeuw-van Dalfsen et al. (2013) showed that in the case of variable compressibility of magma residing in the plumbing system and host rocks, the strain change in the crust can be accommodated without producing detectable surface deformation. Further work is needed to provide additional constraints to the observed deflation, for example, seismological observations to outline the pathways for mass transportation and micro-gravity observations to confine the magnitude of the possible mass relocation.

5.2. Great Sitkin

Two explosive eruptions were produced at Great Sitkin from the center crater in 2018 and 2021. The 2018 event started in June 2018 and ended in December 2018. The 2021 eruption started in May 2021 and has been characterized by sustained, slow lava effusions as of October 2023. With both these two eruptions captured in our InSAR observation period, we have identified one inflation episode that initiated around September 2018 and peaked around September 2020, and then diminished rapidly around October 2021. The inflation can be well reproduced by a Mogi source located ~800 m south and ~1.5 km west of the caldera center at a depth of about 5–7 km BSL, with a volume change rate of about 5.4×10^6 m^3/yr (Figure S4 in Supporting Information S1).

The inflating Mogi source from 2018 to 2020 is most likely indicative of magma accumulation in the magma chamber below the summit caldera that fed the 2021 eruption. Pesicek et al. (2008) identified a low P wave velocity region with appreciable thickness extending from the surface to ~10 km depth beneath the summit caldera, with shallow earthquakes (<5 km) spread in a wide depth range within a small region beneath the summit. The shallow part (<5 km) of the low P-wave velocity region with high seismicity concentration and shallow long-period (LP) events is interpreted as the active hydrothermal system of Great Sitkin. The deeper part (>5 km) of the low P-wave velocity region is suggested to be a region with high-temperature anomaly and/or partially molten rock which may represent the magma storage (Pesicek et al., 2008). The location and depth of this low P-wave velocity zone are highly consistent with the Mogi source derived from our InSAR observation. Deep LP events have also been recorded at Great Sitkan in Power et al. (2004), in which the deep LP events are suggested to represent magma ascent from the upper mantle or lower crust to feed a shallow magma chamber. From 2015 to 2021, several seismic swarms were detected mainly in a NW-SE trending zone at Great Sitkin, distributed in a cap-like zone across the summit caldera (Figure S5 in Supporting Information S1). The deeper area (>5 km) with sparse seismicity capped by the seismic swarms may represent the region of the proposed magma reservoir. The shallow seismic swarms beneath the caldera concentrated from 2018 to 2020 may represent the elevated hydrofluid-magma interaction during the magma accumulation. The earthquake swarm right beneath the caldera in 2021 may be indicative of the rupture of the host rock surrounding the magma reservoir and the migration of the magma along the conduit. The deflation starting in August 2021 is consistent with the onset of the 2021 eruption. Furthermore, the volume of the lava dome produced during the 2021 eruption is estimated to have a volume of $\sim 2.4 \times 10^7$ m^3 by October 2021 (https://avo.alaska.edu/activity/report.php?type=4&id=395381&mode=hans), which is close to the modeled volume loss in 2021 from InSAR ($\sim 1.5 \times 10^7$ m^3, Figure 2g). It is also worth noting that persistent volume increase is observed even during the 2018 eruption, considering the phreatic nature of the 2018 eruption and the high seismicity rate between the 2018 and 2021 eruptions, we presume that both the two eruptions pertain to the same unrest cycle.

5.3. Tanaga

The Tanaga volcanic center is comprised of three young stratovolcanoes, that is, Sajaka in the west, Tanaga in the middle, and Takawangha in the east. During October–November 2005, caldera-wide inflation centered between

the Tanaga and Takawangha volcanoes was found accompanied by seismic unrest and was modeled as pressurization in a shallow dipping prolate spheroid source located about 3–5 km BSL (Lu & Dzurisin, 2014). In our InSAR observation, a large-scale transient deformation that occurred between November 2019 and August 2020 is found covering the whole northeastern part of Tanaga island, aligned near west-east with the northern part moving to the east and the southern part moving toward the west. The best-fit model is a nearly vertically dipping strike-slip fault located 10 km east and 2,500 m north to the Takawangha caldera, striking to ∼80° clockwise to the north at a depth of ∼4 km BSL, with a length of ∼11 km, a width of ∼600 m and slip of ∼4 m (Figure S6 in Supporting Information S1).

According to the USGS Comprehensive Earthquake Catalog (ComCat), several large swarms of earthquakes have been recorded in the E-SE of Takawangha from 2015 to 2021 (Figure S7 in Supporting Information S1). The 2020 earthquake swarm struck a large area extending from the peak of Takawangha to about 24 km to the N-NE, with more than 1,000 events distributed at depths ranging from 18 km BSL to the surface. This seismic swarm coincides spatially with the deformation signal. Another seismic swarm between January 24 to 27 of 2017 includes about 100 events and is mainly distributed in a depth range of 4–12 km BSL. The shallowing depth trend with time may be indicative of stress perturbation due to the migration of magma or hydrofluid in cracks. The distribution of seismic clusters is consistent with the N70° trend of possible magma paths derived from morphometric characteristics of the Tanaga volcanic center, which likely played a critical role in the activation of the large-scale strike-slip events in 2020 (Tibaldi & Bonali, 2017). Furthermore, the temporal distribution of seismic moment release, derived by converting the magnitude from local magnitude M_l and body-wave magnitude m_b to moment magnitude M_w using the imperial relation in Ruppert and Hansen (2010), shows very high moment concentrations in January 2020 (Figure S8 in Supporting Information S1). This is coeval with the occurrence of the transient deformation and is very likely accounting for the energy needed to produce the large-scale deformation. The strike angle and slip direction of the modeled fault are highly consistent with the nearby M5.0 and M6.6 earthquakes that occurred between Tanaga Volcano to the west and Kanaga Volcano to the east in May 2008 (Ruppert et al., 2012), suggesting the seismic swarm is a result of regional tectonics instead of magmatism. The strike-slip faulting may have been activated by stress perturbation or the presence of possible hydrofluid. Further investigation into the earthquake swarms and local fault information is needed to produce a better understanding of tectonic processes in this area.

6. Conclusions

Advanced cloud-based ARIA-HyP3 InSAR processing has been used to map the surface deformation history for the western and central Aleutian volcanoes. The ARIA tools and OpenSARlab cloud-based utilities remarkably reduce the computational resources and workflows for time-series deformation mapping over a large region. The framework shows great capability in capturing regional volcanic/nonvolcanic deformation with promising accuracy in challenging areas, providing a new option to better explore the value of both the archived and coming SAR data for the science community. The mapped deformation time series of the western and central Aleutian volcanoes show diverse spatial and temporal patterns and variations, suggesting that the magmatic plumbing systems and tectonic settings along the arc are inherently complicated. An overall higher magmatism observed at the central Aleutian volcanoes is identified, and may imply higher magma production rates or ascent rates as a result of regional tectonic settings. Most of the investigated volcanoes exhibit deformation identical to the historically observed patterns in previous studies, indicating similar magmatic activity occurring in their plumbing systems. New deformation patterns have been revealed at Tanaga, Great Sitkin and Yunaska, greatly enriching our knowledge of the spectrum of volcanism in the Aleutian arc. Transient deformation at Tanaga is suggested to be a result of multiple strike-slip earthquakes in response to regional tectonics. The 2018 eruption at Great Sitkin is interpreted as a result of magmatic reservoir rupture which accommodated lava dome emplacement during the 2021 eruption. The continuous deflation at Yunaska is speculated to be a consequence of magma withdrawal induced by the regional extensional tectonic setting. Updates on arc-wide volcanism are critical for further understanding of magmatism and tectonism, as well as volcanic hazard monitoring and mitigation.

Data Availability Statement

All data sets used in this study are publicly available. The ARIA-GUNW products can be accessed from the ASF DAAC. ARIA-tools and MintPy are used to produce the deformation time series (Bekaert et al., 2019; Zhang et al., 2019). PyAPS is used for APS correction (Jolivet et al., 2011). The EAR5 data are provided by

ECMWF (https://www.ecmwf.int/en/forecasts/datasets/reanalysis-datasets/era5). GNSS data are processed by the Nevada Geodetic Laboratory (http://geodesy.unr.edu/) (Blewitt et al., 2018). Earthquake data are available at U.S. Geological Survey (USGS; https://earthquake.usgs.gov/data/comcat/). GBIS is used for deformation source inversion (Bagnardi & Hooper, 2018). Volcano eruption histories are provided by Alaska Volcano Observatory (AVO; https://avo.alaska.edu/volcanoes/index.php). InSAR deformation velocity and modeling results are available at "Figshare" (https://doi.org/10.6084/m9.figshare.22817780).

Acknowledgments
We thank the ARIA-HYP3 team for producing the ARIA-GUNW data. This work was supported through the "enabling cloud based InSAR science" ACCESS 2019 award. Part of this work was carried out at the Jet Propulsion Laboratory, California Institute of Technology, under a contract with the National Aeronautics and Space Administration. J. Wang, Z. Lu and P. Gregg were also supported by NASA Earth & Surface Interior Program (80NSSC19K0357). Constructive comments from Editor Prof. Lucy Flesch, Prof. Xiaohua Xu and an anonymous reviewer significantly improved the manuscript.

References

Bagnardi, M., & Hooper, A. (2018). Inversion of surface deformation data for rapid estimates of source parameters and uncertainties: A Bayesian approach [Software]. Geochemistry, Geophysics, Geosystems, *19*, 2194–2211. https://doi.org/10.1029/2018gc007585

Bekaert, D., Walters, R. J., Wright, T. J., Hooper, A. J., & Parker, D. J. (2015). Statistical comparison of InSAR tropospheric correction techniques. *Remote Sensing of Environment*, *170*, 40–47. https://doi.org/10.1016/j.rse.2015.08.035

Bekaert, D. P., Karim, M., Linick, J. P., Hua, H., Sangha, S., Lucas, M., et al. (2019). Development of open-access standardized InSAR displacement products by the advanced rapid imaging and analysis (ARIA) project for natural hazards [Software]. AGU Fall Meeting Abstracts. Retrieved from https://ui.adsabs.harvard.edu/abs/2019AGUFM.G23A..04B/abstract

Berardino, P., Fornaro, G., Lanari, R., & Sansosti, E. (2002). A new algorithm for surface deformation monitoring based on small baseline differential SAR interferograms. *TGRS*, *40*(11), 2375–2383. https://doi.org/10.1109/TGRS.2002.803792

Blewitt, G., Hammond, W. C., & Kreemer, C. (2018). Harnessing the GPS data explosion for interdisciplinary science [Dataset]. Eos, *99*(1029). 485. https://doi.org/10.1029/2018eo104623

Buurman, H., Nye, C. J., West, M. E., & Cameron, C. (2014). Regional controls on volcano seismicity along the Aleutian arc. *Geochemistry, Geophysics, Geosystems*, *15*(4), 1147–1163. https://doi.org/10.1002/2013GC005101

Buzzanga, B., Bekaert, D. P. S., Hamlington, B. D., & Sangha, S. S. (2020). Toward sustained monitoring of subsidence at the coast using InSAR and GPS: An application in Hampton roads, Virginia. *Geophysical Research Letters*, *47*(18), e2020GL090013. https://doi.org/10.1029/2020gl090013

Chen, C. W., & Zebker, H. A. (2002). Phase unwrapping for large SAR interferograms: Statistical segmentation and generalized network models. *IEEE Transactions on Geoscience and Remote Sensing*, *40*(8), 1709–1719. https://doi.org/10.1109/tgrs.2002.802453

de Zeeuw-van Dalfsen, E., Rymer, H., Sigmundsson, F., & Sturkell, E. (2005). Net gravity decrease at Askja volcano, Iceland: Constraints on processes responsible for continuous caldera deflation, 1988–2003. *Journal of Volcanology and Geothermal Research*, *139*(3), 227–239. https://doi.org/10.1016/j.jvolgeores.2004.08.008

de Zeeuw-van Dalfsen, E., Rymer, H., Sturkell, E., Pedersen, R., Hooper, A., Sigmundsson, F., & Ófeigsson, B. (2013). Geodetic data shed light on ongoing caldera subsidence at Askja, Iceland. *Bulletin of Volcanology*, *75*(5), 1–13. https://doi.org/10.1007/s00445-013-0709-2

DeMets, C., Gordon, R. G., Argus, D. F., & Stein, S. (1994). Effect of recent revisions to the geomagnetic reversal time scale on estimates of current plate motions. *Geophysical Research Letters*, *21*(20), 2191–2194. https://doi.org/10.1029/94GL02118

Dzurisin, D., Lu, Z., Poland, M. P., & Wicks, C. W. (2019). Space-based imaging radar studies of U.S. Volcanoes. *Frontiers in Earth Science*, *6*. https://doi.org/10.3389/feart.2018.00249

Fattahi, H., & Amelung, F. (2014). InSAR uncertainty due to orbital errors. *Geophysical Journal International*, *199*(1), 549–560. https://doi.org/10.1093/gji/ggu276

Fischer, T. P., Lopez, T. M., Aiuppa, A., Rizzo, A. L., Ilanko, T., Kelley, K. A., & Cottrell, E. (2021). Gas emissions from the western Aleutians volcanic arc. *Frontiers in Earth Science*, *9*, 9. https://doi.org/10.3389/feart.2021.786021

Geist, D. J., Harpp, K. S., Naumann, T. R., Poland, M., Chadwick, W. W., Hall, M., & Rader, E. (2008). The 2005 eruption of Sierra Negra volcano, Galápagos, Ecuador. *Bulletin of Volcanology*, *70*(6), 655–673. https://doi.org/10.1007/s00445-007-0160-3

Gong, W., Meyer, F. J., Lee, C.-, Lu, Z., & Freymueller, J. (2015). Measurement and interpretation of subtle deformation signals at Unimak Island from 2003 to 2010 using weather model-assisted time series InSAR. *Journal of Geophysical Research: Solid Earth*, *120*(2), 1175–1194. https://doi.org/10.1002/2014JB011384

Hamling, I. J., Wright, T. J., Calais, E., Lewi, E., & Fukahata, Y. (2014). InSAR observations of post-rifting deformation around the Dabbahu rift segment, Afar, Ethiopia. *Geophysical Journal International*, *197*(1), 33–49. https://doi.org/10.1093/gji/ggu003

Jolivet, R., Grandin, R., Lasserre, C., Doin, M.-, & Peltzer, G. (2011). Systematic InSAR tropospheric phase delay corrections from global meteorological reanalysis data [Software]. Geophysical Research Letters, *38*(17), L17311. https://doi.org/10.1029/2011GL048757

Kelemen, P. B., Yogodzinski, G. M., & Scholl, D. W. (2003). Along-strike variation in lavas of the Aleutian island arc: Implications for the genesis of high Mg# andesite and the continental crust, inside the subduction factory. *Geophysical Monograph*, *138*, 223–276.

Kiyoo, M. (1958). Relations between the eruptions of various volcanoes and the deformations of the ground surfaces around them. *Earthquake Engineering Research Institute*, *36*, 99–134.

Kreemer, C., Blewitt, G., & Klein, E. C. (2014). A geodetic plate motion and global strain rate model. *Geochemistry, Geophysics, Geosystems*, *15*(10), 3849–3889. https://doi.org/10.1002/2014GC005407

Kwoun, O., Lu, Z., Neal, C., & Wicks, C. (2006). Quiescent deformation of the Aniakchak caldera, Alaska, mapped by InSAR. *Geology*, *34*(1), 5–8. https://doi.org/10.1130/G22015.1

Lee, C., Lu, Z., Won, J., Jung, H., & Dzurisin, D. (2013). Dynamic deformation of Seguam Island, Alaska, 1992–2008, from multi-interferogram InSAR processing. *Journal of Volcanology and Geothermal Research*, *260*, 43–51. https://doi.org/10.1016/j.jvolgeores.2013.05.009

Lee, J., Papathanassiou, K. P., Ainsworth, T. L., Grunes, M. R., & Reigber, A. (1998). A new technique for noise filtering of SAR interferometric phase images. *IEEE Transactions on Geoscience and Remote Sensing*, *36*(5), 1456–1465. https://doi.org/10.1109/36.718849

Li, Z., Fielding, E. J., & Cross, P. (2009). Integration of InSAR time-series analysis and water-vapor correction for mapping postseismic motion after the 2003 Bam (Iran) earthquake. *TGRS*, *47*(9), 3220–3230. https://doi.org/10.1109/TGRS.2009.2019125

Lu, Z., & Dzurisin, D. (2010). Ground surface deformation patterns, magma supply, and magma storage at Okmok volcano, Alaska, from InSAR analysis: 2. Coeruptive deflation, July-August 2008. *Journal of Geophysical Research*, *115*(B5), B00B03. https://doi.org/10.1029/2009JB006970

Lu, Z., & Dzurisin, D. (2014). *InSAR imaging of Aleutian volcanoes*. Springer.

Lu, Z., Dzurisin, D., Biggs, J., Wicks, C., Jr., & McNutt, S. (2010). Ground surface deformation patterns, magma supply, and magma storage at Okmok volcano, Alaska, from InSAR analysis: 1. Intereruption deformation, 1997–2008. *Journal of Geophysical Research*, *115*(B5), B00B02. https://doi.org/10.1029/2009jb006969

Lu, Z., Masterlark, T., Dzurisin, D., Rykhus, R., & Wicks, C., Jr. (2003). Magma supply dynamics at Westdahl volcano, Alaska, modeled from satellite radar interferometry. *Journal of Geophysical Research*, *108*(B7), 2354–n/a. https://doi.org/10.1029/2002JB002311

Magee, C., Jackson, C. A. L., & Schofield, N. (2013). The influence of normal fault geometry on igneous sill emplacement and morphology. *Geology*, *41*(4), 407–410. https://doi.org/10.1130/G33824.1

Mann, D., & Freymueller, J. (2003). Volcanic and tectonic deformation on Unimak Island in the Aleutian arc, Alaska. *Journal of Geophysical Research*, *108*(B2), 2108. https://doi.org/10.1029/2002JB001925

Meyer, F. J., Rosen, P. A., Flores, A., Anderson, E. R., & Cherrington, E. A. (2021). Making sar accessible: Education & training in preparation for Nisar. In *2021 IEEE international geoscience and remote sensing symposium IGARSS*.

Nakaboh, M., Ono, H., Sako, M., Sudo, Y., Hashimoto, T., & Hurst, A. W. (2003). Continuing deflation by fumaroles at Kuju volcano, Japan. *Geophysical Research Letters*, *30*(7), 1396–n/a. https://doi.org/10.1029/2002GL016047

Ofeigsson, B. G., Hooper, A., Sigmundsson, F., Sturkell, E., & Grapenthin, R. (2011). Deep magma storage at Hekla volcano, Iceland, revealed by InSAR time series analysis. *Journal of Geophysical Research*, *116*(B5), B05401. https://doi.org/10.1029/2010JB007576

Pesicek, J. D., Thurber, C. H., DeShon, H. R., Prejean, S. G., & Zhang, H. (2008). Three-dimensional P-wave velocity structure and precise earthquake relocation at Great Sitkin Volcano, Alaska. *Bulletin of the Seismological Society of America*, *98*(5), 2428–2448. https://doi.org/10.1785/0120070213

Power, J. A., Stihler, S. D., White, R. A., & Moran, S. C. (2004). Observations of deep long-period (DLP) seismic events beneath Aleutian arc volcanoes; 1989–2002. *Journal of Volcanology and Geothermal Research*, *138*(3), 243–266. https://doi.org/10.1016/j.jvolgeores.2004.07.005

Rosen, P. A., Gurrola, E., Sacco, G. F., & Zebker, H. (2012). The InSAR scientific computing environment. In *EUSAR 2012; 9th European conference on synthetic aperture radar*.

Ruppert, N. A., & Hansen, R. A. (2010). Temporal and spatial variations of local magnitudes in Alaska and Aleutians and comparison with body-wave and moment magnitudes. *Bulletin of the Seismological Society of America*, *100*(3), 1174–1183. https://doi.org/10.1785/0120090172

Ruppert, N. A., Kozyreva, N. P., & Hansen, R. A. (2012). Review of crustal seismicity in the Aleutian Arc and implications for arc deformation. *Tectonophysics*, *522–523*, 150–157. https://doi.org/10.1016/j.tecto.2011.11.024

Rymer, H., Cassidy, J., Locke, C. A., & Sigmundsson, F. (1998). The 1998 debris avalanche at Casita volcano, Nicaragua – Investigation of structural deformation as the cause of slope instability using remote sensing. *Journal of Volcanology and Geothermal Research*, *87*(1–4), 141–149. https://doi.org/10.1016/S0377-0273

Sangha, S. S. (2021). *Characterizing the deformation field in Afar from radar interferometry and topography data*. University of California.

Shreve, T., Grandin, R., & Boichu, M. (2022). Reservoir depressurization driven by passive gas emissions at Ambrym volcano. *Earth and Planetary Science Letters*, *584*, 117512. https://doi.org/10.1016/j.epsl.2022.117512

Tibaldi, A., & Bonali, F. L. (2017). Intra-arc and back-arc volcano-tectonics: Magma pathways at Holocene Alaska-Aleutian volcanoes. *Earth-Science Reviews*, *167*, 1–26. https://doi.org/10.1016/j.earscirev.2017.02.004

Tibaldi, A., Pasquarè, F., & Tormey, D. (2010). Volcanism in reverse and strike-slip fault settings. *New Frontiers in Integrated Solid Earth Sciences*, 315–348. https://doi.org/10.1007/978-90-481-2737-5_9

Townsend, M. (2022). Linking surface deformation to thermal and mechanical magma chamber processes. *Earth and Planetary Science Letters*, *577*, 117272. https://doi.org/10.1016/j.epsl.2021.117272

Trasatti, E., Acocella, V., Di Vito, M. A., Del Gaudio, C., Weber, G., Aquino, I., et al. (2019). Magma Degassing as a source of long-term seismicity at volcanoes: The Ischia Island (Italy) case. *Geophysical Research Letters*, *46*(24), 14421–14429. https://doi.org/10.1029/2019GL085371

Wang, J., Lu, Z., & Gregg, P. M. (2021). Inflation of Okmok volcano during 2008–2020 from PS analyses and source inversion with finite element models. *Journal of Geophysical Research: Solid Earth*, *126*(10), e2021JB022420. https://doi.org/10.1029/2021jb022420

Wang, T., DeGrandpre, K., Lu, Z., & Freymueller, J. T. (2018). Complex surface deformation of Akutan volcano, Alaska revealed from InSAR time series. *International Journal of Applied Earth Observation and Geoinformation*, *64*, 171–180. https://doi.org/10.1016/j.jag.2017.09.001

Wang, T., Poland, M. P., & Lu, Z. (2015). Dome growth at Mount Cleveland, Aleutian Arc, quantified by time series TerraSAR-X imagery. *Geophysical Research Letters*, *42*(24), 10614–10621. https://doi.org/10.1002/2015GL066784

Wang, X., & Aoki, Y. (2019). Posteruptive thermoelastic deflation of intruded magma in Usu volcano, Japan, 1992–2017. *Journal of Geophysical Research: Solid Earth*, *124*(1), 335–357. https://doi.org/10.1029/2018jb016729

Xue, X., & Freymueller, J. T. (2020). A 25-year history of volcano magma supply in the east central Aleutian arc, Alaska. *Geophysical Research Letters*, *47*(15), e2020GL088388. https://doi.org/10.1029/2020gl088388

Zhang, Y., Fattahi, H., & Amelung, F. (2019). Small baseline InSAR time series analysis: Unwrapping error correction and noise reduction [Software]. Computers & Geosciences, *133*, 104331. https://doi.org/10.1016/j.cageo.2019.104331